Inhomogeneous spinel in chromitite from the Iwanai-dake peridotite complex, Hokkaido, Japan : variations of spinel unmixing texture and chemical composition

Sci. Rep. Kanazawa Univ.
Vol.48, No.1,2, p.9-29, 2004

Inhomogeneous spinel in chromitite from the Iwanai-dake peridotite complex, Hokkaido, Japan: variations of spinel unmixing texture and chemical composition

Akihiro TAMURA[1] and Shoji ARAI[2]

1 Graduate School of Natural Science and Technology, Kanazawa University, Kakuma, Kanazawa 920-1192, Japan
2 Department of Earth Sciences, Kanazawa University, Kakuma, Kanazawa 920-1192, Japan

Abstract : Spinel ($(Mg\ Fe^{2+})(Cr\ Al\ Fe^{3+})_2O_4$ in formula) with inhomogeneous textures were observed in chromitite from the Iwanai-dake complex, in the Kamuikotan zone, Japan, which mainly consists of highly depleted alpine-type peridotite. The spinel inhomogeneous texture is different between in the chromitite layer and in the surrounding peridotites but the variation is gradual. Spinel has a speckled texture (Type A spinel) in the chromitite. Irregular mottling and symplectic textures (Type B spinel) are predominant in spinel-rich dunite abutting to the chromitite layer. Spinel in the surrounding dunite and harzburgite is homogeneous (Type C spinel), and it is similar in composition to spinel in ordinary peridotite from the Iwanai-dake complex. The inhomogeneous spinel comprises two phases of Mg-and Al-rich spinel and Fe^{2+}-and Fe^{3+}-rich spinel. The variations of texture and composition were achieved by an unmixing process due to the miscibility gap of spinel between the Al-rich and Fe^{3+}-rich phases below 900°C. The Iwanai-dake peridotite is almost free from serpentinization and lacks evidence of regional metamorphism after emplacement, which suggests that the unmixing of spinel took place during a cooling process of the mantle peridotite. The pre-unmixing compositions of Type A and B spinels are estimated as bulk spinel compositions, and they are systematically correlated with the unmixing texture. We propose that the variation of unmixing texture is controlled by pre-unmixing spinel compositions.

1. Introduction

Spinel group minerals have a wide range of composition reflecting various chemical and physical conditions of their genesis. Spinel, $(Mg, Fe^{2+})(Cr, Al, Fe^{3+})_2O_4$, is especially employed as a useful petrogenetic indicator for ultramafic and mafic rocks because its composition is sensitive to change of temperature, pressure, oxygen fugacity, bulk rock and fluid compositions (e.g., Irvine, 1965). For upper mantle-derived peridotites, its composition may indicate the degree of partial melting and has been used as a guide to classification of peridotites in terms of tectonic setting (e.g., Dick and Bullen, 1984 ; Arai, 1994). Although the extensive solid solution exists in spinel group minerals at high temperatures

such as upper mantle conditions, miscibility gaps between aluminum-and ferric iron-rich spinels are recognized at lower temperatures such as greenschist, amphibolite or granulite facies condition (e.g., Loferski and Lipin, 1983). The experimental and thermodynamic studies have shown a solvus between them (Turnock and Eugster, 1962 ; Cremer, 1969 ; Sack and Ghiorso, 1991). Spinels with a miscibility gap often develop unmixing textures as described from metamorphosed ultramafic and mafic rocks (Muir and Naldrett, 1973 ; Loferski and Lipin, 1983 ; Lipin, 1984 ; Eales et al., 1988 ; Zakrezewski, 1989 ; Burkhard, 1993). Loferski and Lipin (1983) referred to the scarcity of unmixing spinels from mantle derived peridotites. Unmixing-textured spinels have been reported only from alpine -type peridotite that has undergone regional crustal metamorphism (Lipin, 1984 ; Burkhard, 1993). We found inhomogeneous spinels from a chromitite layer in a mantle-derived peridotite complex, the Iwanai-dake complex, Hokkaido, northern Japan. In this article we describes textural and compositional characteristics of the inhomogeneous spinel. Then we show that the inhomogeneous texture of spinel is caused by unmixing during cooling of mantle peridotite and that pre-unmixing spinel compositions control the unmixing texture. In this article, "spinel" refers to a spinel group mineral generally expressed as $(Mg, Fe^{2+})(Cr, Al, Fe^{3+})_2 O_4$ (e.g., Haggerty, 1991a). "Chromitite" refers to the rock rich in "spinel" (> 20% modal ratio) defined above.

2. Geology and petrology of the Iwanai-dake peridotite complex

The Iwanai-dake peridotite complex is located in the southern part of the Kamuikotan zone. The Kamuikotan zone is distributed discontinuously over 320 km from north to south within the Sorachi-Yezo belt of a Mesozoic accretionary complex, the central axial zone of Hokkaido, northern Japan, and is a tectonic melange which consists of peridotites and high-and low-pressure metamorphic rocks (Miyashiro, 1961 ; Ishizuka, 1983). Distribution of a large amount of ultramafic rocks serpentinized to various degrees characterizes the Kamuikotan zone (Fig. 1), and some of them are considered to the basal mantle member of an ophiolite complex (e.g., Asahina and Komatsu, 1979 ; Ishizuka, 1980 ; Ishizuka et al., 1983). The Iwanai-dake complex, approximately 2 km X 0.5 km in plan, is mainly composed of spinel harzburgite and dunite with a small amount of pyroxenites (orthopyroxenite or olivine-orthopyroxenite) and chromitite. They are well exposed at a large quarry around Mt. Iwanai-dake (964 m) and are almost free from serpentinization (Bamba, 1955 ; Arai, 1978 ; Katoh, 1978 ; Niida and Katoh, 1978). Dunite commonly forms tabular layers or veins that range in thickness from 10 cm to 10 m within massive harzburgite (e.g. Tamura et al., 1999 ; Kubo, 2002). Layers or veins of pyroxenite and chromitite are associated with dunite in places. The harzburgite and dunite have strong deformed textures with kink-banded olivine, such as protogranular and porphyroclastic textures of Mercier and Nicolas (1975). Relics of fluid inclusions (Arai and Hirai, 1985 ; Hirai and Arai, 1987), chromian spinel lamellae (Arai, 1978) and fine inclusions in the olivine grains are much more frequently found in dunite than in harzburgite. The compositional variations of

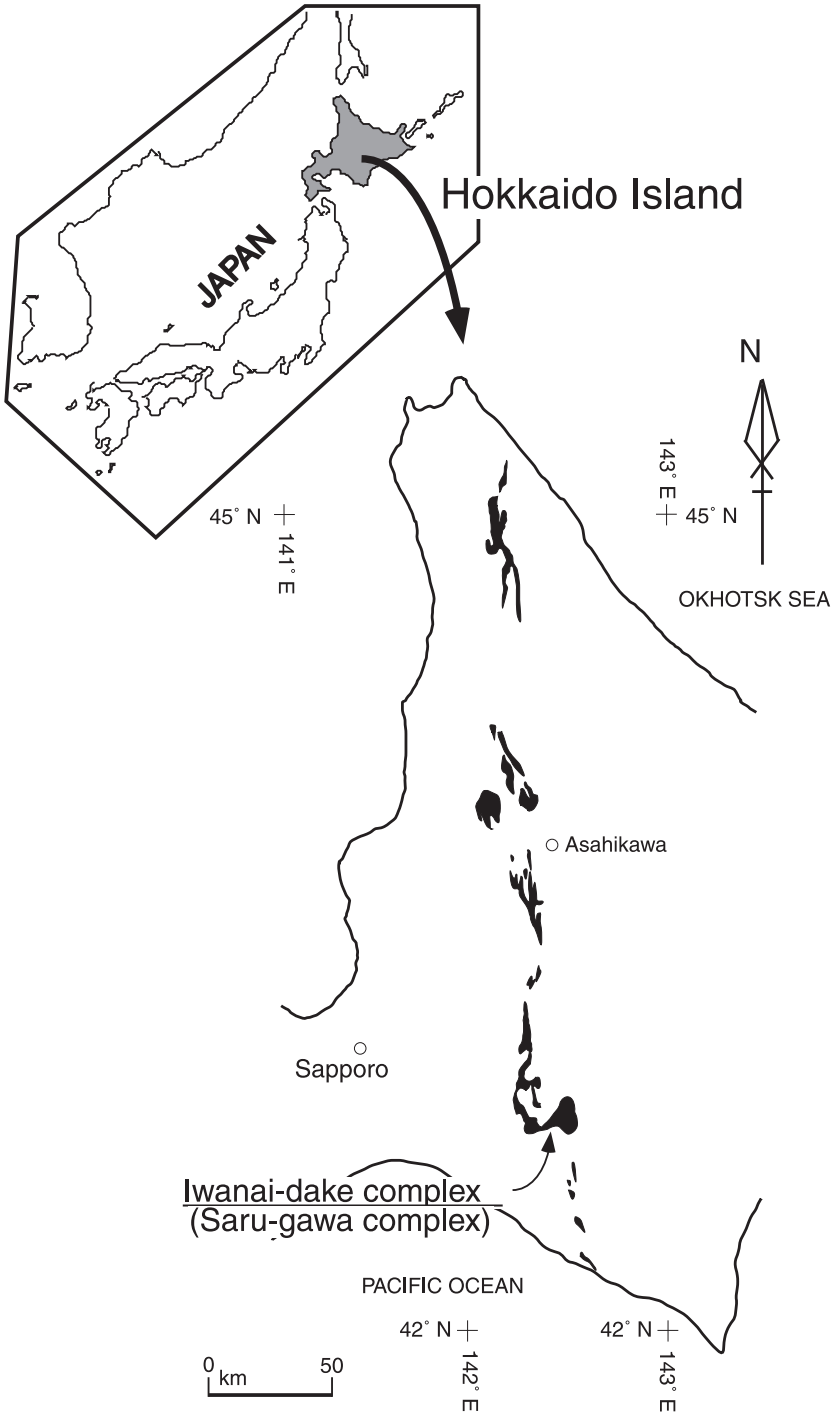

Figure. 1. Locality of the Iwanai-dake peridotite complex and distribution of the ultramafic rocks in the Kamuikotan zone, Hokkaido, northern Japan.

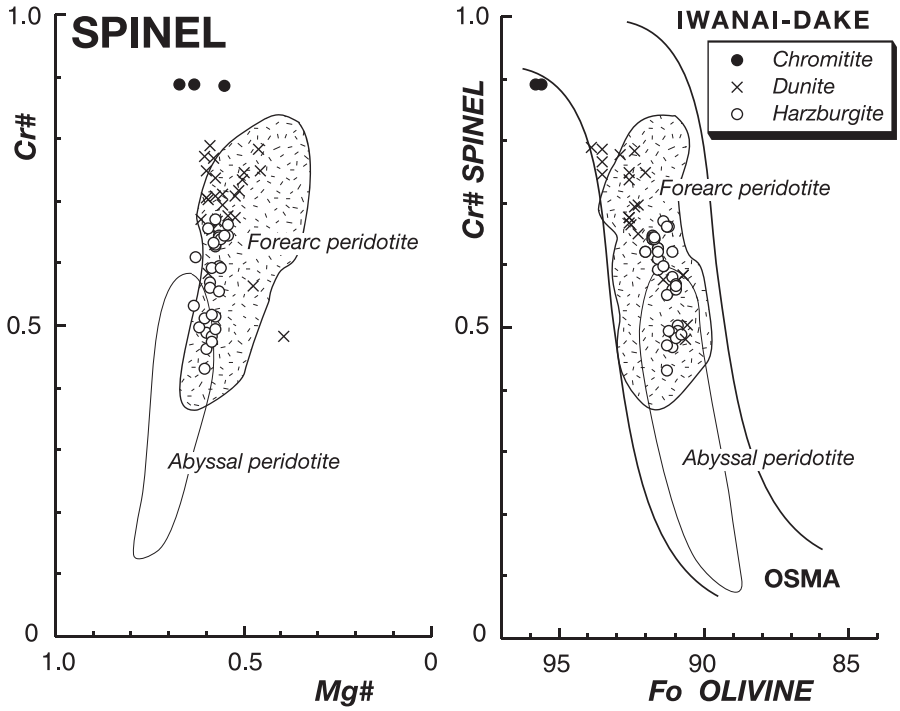

Figure. 2. Chemical compositions of spinel and olivine in ordinary peridotite and chromitite from the Iwanai-dake complex. Abyssal peridotite field from Dick and Bullen (1984) and Arai (1994). Forearc peridotite field from Bloomer and Hawkins (1983), Bloomer and Fisher (1987), Ishii et al. (1992) and Parkinson and Pearce (1998). (a) Mg# (=Mg/(Mg+Fe^{2+}) atomic ratio) vs Cr# (=Cr/(Cr+Al) atomic ratio) of spinel. (b) Fo content of olivine vs Cr# of spinel. Note that, for coexisting chromian spinel-olivine pairs in harzburgite and dunite, the Cr# and Fo content have a positive correlation entirely along the olivine-spinel mantle array (OSMA : Arai, 1987, 1994), a spinel peridotite restite trend.

olivine and spinel in peridotite and chromitite are illustrated in Figure 2. The Iwanai-dake peridotite is characteristically depleted and is similar in mineral chemistry to forearc peridotites rather than to abyssal peridotites (Fig. 2).

3. Studied chromitite

The studied rocks were obtained from a chromitite layer and surrounding peridotites at the eastern part (outcrop No. IWD580) of the quarry. The lithological sequence of IWD 580 is illustrated in Figure 3a. The samples were collected by drilling up to a distance 100 cm from the chromitite layer into surrounding dunite and harzburgite (Fig. 3a). The chromitite layer, about 5 cm in thickness, appears to be continuous over about 80 cm in length (samples MF5 and 22), and pinches out at one end (Plate I-a,b). Small amounts of subhedral olivine (up to 5 mm in diameter) are enclosed by massive spinel. The boundary between chromitite and dunite is clearly identified as grain boundaries between massive spinel aggregate and olivine (Fig. 3b). The abutting dunite layers (5 cm in thickness) en-

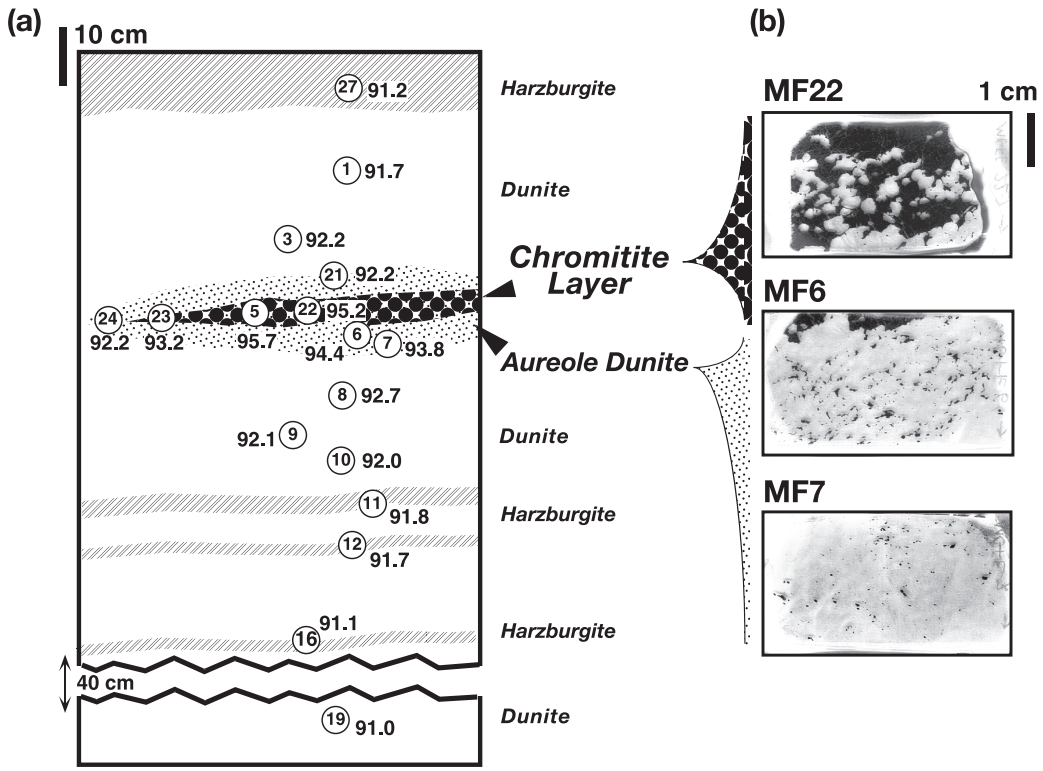

Figure. 3. (a) Sketch of studied section (IWD580). Sample numbers encircled are shown with Fo content of olivine. See plate I-a and b for outcrop. (b) The variation from chromitite layer to aureole dunite is shown by the thin sections of MF 22, 6 and 7. Black stuff is spinel and a light grey is almost olivine. Note the antinodular texture in chromitite (MF22) and a decrease of spinel volume within the aureole dunite (MF6 and 7) from chromitite border toward surrounding dunite.

closing the chromitite layer are richer in spinel than the surrounding dunite and harzburgite, and are called aureole dunite hereafter (samples MF6, 7, 21, 23 and 24) (Fig. 3a). In the aureole dunite subhedral and anhedral spinel grains (0.1-1.0 mm in diameter) are interstitial to olivine, and minor amount of chlorite (clinochlore) and andradite are also interstitial to olivine and/or spinel. It is noteworthy that andradite sometimes occurs in the core of chlorite. Spinel volume is gradually decreasing with an increase of distance from the chromitite layer. The Surrounding dunite (samples MF1, 3, 8, 9, 10 and 19) and harzburgite (samples MF11, 12, 16 and 27), which are peridotites outside of the aureole dunite, are similar to ordinary peridotites from the Iwanai-dake complex. The massive spinel aggregate in the chromitite layer is usually black with translucent yellow or green blebs in thin section (Plate I-c). Kink band of olivine is less frequent in chromitite than in aureole dunite. The surrounding dunite and harzburgite have a porphyroclastic texture with fairly deformed olivine and orthopyroxene porphyroclasts. Spinels show a range of color from dark brown to light reddish-brown.

4. Spinel textures

Textural and compositional varieties of spinel have been identified by reflected-light microscopic observations (Plate I-IV). In order to simplify the varieties, which are so complicated and gradual, we divided the textures into three types ; Types A and B showing two, dark-colored and light-colored, phases, and Type C with a homogeneous appearance. Type A spinel exhibits a speckled texture consisting of a large amount of dark-colored granules and a light-colored host (e.g., Plate. I-d, e, II-a, IV-a). The granules are often distributed in linear or concentric arrays. Individual granules are rounded to rectangular and range from less than 5 μm to 50 μm in diameter. Type B spinel shows irregular mottling or symplectic texture composed of dark-colored and light-colored phases (e.g., Plate II-e, g, III-a, e, IV-b). Gradual change of the inhomogeneous texture is achieved by change of the ratio of the two phases. Symplectic-textured part sometimes coexists with apparently homogeneous part within single spinel grains (e.g., Plate. III-c, g, IV-c). Type C is mainly composed of a dark-colored phase (e.g., Plate IV-g, h) but some of Type C grains are zoned in dunite aureole (e.g., Plate. III-h, IV-f). Type A spinel is mainly observed in the chromitite layer. Within the aureole dunite, the dominant spinel type changes in the order of Type A, B, C from chromitite border outward. Only Type C spinel occurs in the surrounding dunite and harzburgite. We summarize that the textural variation of spinel is related not only to lithology of host rock but also to distance from the chromitite layer.

5. Mineral chemistry

Chemical analysis of minerals were carried out with an energy dispersive spectrometer system (Phillips EDAX-9100) attached to scanning electron microscope (AKASHI ALPHA-30A) at Faculty of Science, Kanazawa University and with a wavelength dispersive spectrometer system (JEOL EPMA JXA-8800) at Center for Cooperative Research of Kanazawa University. In the microprobe analysis of spinel, Fe is reported as total FeO, and Fe^{2+} and Fe^{3+} were recalculated by assuming ideal spinel stoichiometry with all Ti being allotted to ulvospinel (Fe_2TiO_4). Both Fe_2O_3 and FeO were recalculated along with the resulting new totals. Selected analyses of spinel are listed in Table 1. Figures 4, 5 and 6 illustrate the compositional relationships between Type A, B and C spinels. The dark-colored phase is rich in the component of spinel *sensu stricto* ($MgAl_2O_4$) whereas the light-colored phase is intermediate between magnetite ($Fe^{2+}Fe^{3+}{}_2O_4$) and magnesioferrite ($MgFe^{3+}{}_2O_4$) components (Figs. 4 and 5a). The compositional variation of Types A, B and C is dependent on distance from the chromitite layer. For example, within the aureole dunite Type B spinel in chromitite side is lower in chromium content than that in the surrounding peridotite side. TiO_2 contents are usually low (<0.5 wt%) in all spinel phases (Fig. 6a). Some Type B spinels have relatively high TiO_2 content, up to 1 wt%, especially in the light-colored phase. The NiO content of spinel is higher in the chromitite and aureole dunite than in the surrounding dunite and harzburgite (Fig. 6b). Dark-colored and light-colored phases in Type A and B spinels contain 0.10-0.54 wt% and 0.56-1.40 wt% of NiO, respectively. The NiO

Table.1. Representative microprobe analysis of spinels. Refer to Figure 3 for sample#. Total* is a new total from FeO and Fe_2O_3 calculated assuming spinel stoichiometry. †：thin harzburgite layer within dunite. ††=massive harzburgite. Mg#=Mg/(Mg+Fe^{2+}) atomic ratio; Cr#=Cr/(Cr+Al) atomic ratio; R3+= Cr+Al+Fe^{3+}; Fet=Fe^{2+}+Fe^{3+}.

	TYPE A				TYPE B						TYPE C				
Sample#	MF22		MF6		MF6		MF7		MF24		MF7	MF9	MF11	MF19	MF27
Lithology	Chromitite	Chromitite	Aureole	Aureole	Aureole	Aureole	Aureole	Aureole	Aureole	Aureole	Aureole	Dunite	L-Harz†	Dunite	M-Harz††
Point	Host	Granule	Host	Granule	Light	Dark	Light	Dark	Light	Dark	H	SP4	SP2	SP1	SP3
SiO_2	0.00	0.00	0.01	0.03	0.24	0.15	0.00	0.01	0.36	0.34	0.15	0.02	0.01	0.21	0.16
TiO_2	0.29	0.02	0.38	0.05	0.28	0.09	0.97	0.13	0.75	0.28	0.59	0.14	0.06	0.04	0.15
Al_2O_3	1.79	59.81	4.05	51.91	2.59	53.15	4.90	38.82	5.76	22.56	17.04	16.89	21.66	20.04	28.14
Cr_2O_3	2.74	2.74	9.26	11.76	9.57	11.53	17.73	23.23	22.45	28.65	30.94	48.89	48.84	42.47	42.23
Fe_2O_3*	67.13	9.02	57.68	9.06	58.23	5.66	47.56	10.38	40.63	18.32	22.92	6.37	1.12	7.82	0.73
FeO	18.17	2.99	21.00	5.37	22.46	6.74	20.59	8.91	21.37	15.51	16.76	16.31	15.62	18.96	15.20
MnO	0.20	0.05	0.28	0.12	0.35	0.05	0.40	0.23	0.30	0.28	0.36	0.42	0.24	0.37	0.17
MgO	8.16	24.97	6.83	22.92	5.66	21.75	7.09	19.15	6.55	12.45	11.43	12.19	13.09	10.55	14.12
NiO	1.17	0.45	1.25	0.39	1.39	0.34	0.96	0.21	0.57	0.33	0.25	0.08	0.05	0.13	0.00
Total	99.65	100.05	100.77	101.63	100.77	99.45	100.21	101.07	98.74	98.72	100.44	101.33	100.71	100.58	100.90
Si	0.000	0.000	0.000	0.001	0.009	0.004	0.000	0.000	0.013	0.011	0.005	0.000	0.000	0.007	0.005
Ti	0.008	0.000	0.010	0.001	0.008	0.002	0.026	0.003	0.020	0.007	0.014	0.003	0.001	0.001	0.003
Al	0.076	1.769	0.169	1.577	0.110	1.639	0.203	1.266	0.240	0.829	0.639	0.624	0.783	0.743	0.981
Cr	0.078	0.054	0.260	0.240	0.272	0.238	0.492	0.509	0.628	0.707	0.779	1.213	1.185	1.056	0.987
Fe3+	1.818	0.170	1.538	0.176	1.576	0.111	1.259	0.217	1.082	0.434	0.549	0.150	0.026	0.185	0.016
Fe2+	0.547	0.063	0.622	0.116	0.676	0.147	0.606	0.207	0.633	0.409	0.446	0.428	0.401	0.498	0.376
Mn	0.006	0.001	0.008	0.003	0.011	0.001	0.012	0.005	0.009	0.007	0.010	0.011	0.006	0.010	0.004
Mg	0.438	0.934	0.361	0.881	0.303	0.848	0.372	0.790	0.345	0.579	0.542	0.570	0.598	0.495	0.622
Ni	0.034	0.009	0.036	0.008	0.040	0.007	0.027	0.005	0.016	0.008	0.006	0.002	0.001	0.003	0.000
Mg#	0.445	0.937	0.367	0.884	0.310	0.852	0.380	0.793	0.353	0.586	0.549	0.571	0.599	0.498	0.623
Cr#	0.506	0.030	0.605	0.132	0.713	0.127	0.708	0.287	0.723	0.460	0.549	0.659	0.602	0.587	0.502
Cr/R3+	0.039	0.027	0.132	0.120	0.139	0.120	0.252	0.255	0.322	0.359	0.396	0.611	0.594	0.532	0.498
Al/R3+	0.039	0.887	0.086	0.791	0.056	0.824	0.104	0.636	0.123	0.421	0.325	0.314	0.393	0.374	0.494
Fe3+/R3+	0.922	0.085	0.782	0.088	0.805	0.056	0.644	0.109	0.555	0.220	0.279	0.076	0.013	0.093	0.008
Fe3+/Fet	0.769	0.731	0.712	0.603	0.700	0.430	0.675	0.508	0.631	0.515	0.552	0.250	0.060	0.271	0.041

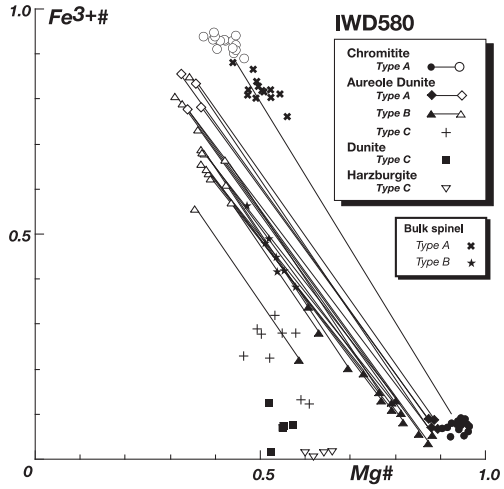

Figure. 4. Mg# (=Mg/(Mg+Fe^{2+}) atomic ratio) vs Fe^{3+}# (=Fe^{3+}/(Cr+Al+Fe^{3+}) atomic ratio) of Type A, B and C spinels from IWD580 in the Iwanai-dake complex. Contiguous pairs of Type A and B spinels are joined by solid line.

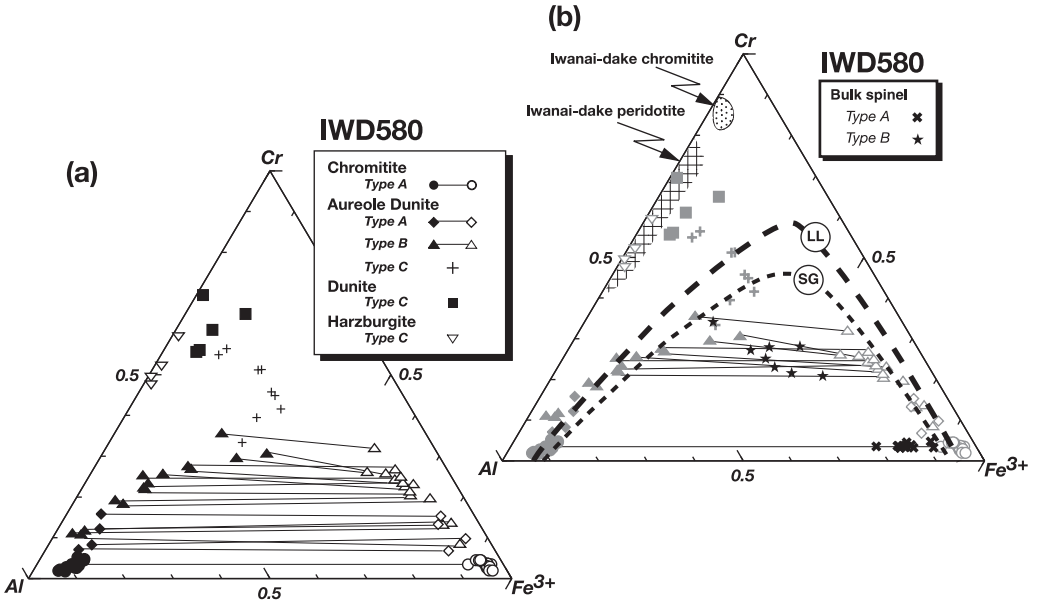

Figure. 5. Compositional relations of Type A, B and C spinels from IWD580 in the Iwanai-dake complex in terms of trivalent cations (Cr, Al and Fe^{3+}). (a) Contiguous pairs of Type A and B spinels are joined by lines. (b) Bulk compositions are estimated from contiguous pairs tied by lines (see text). LL indicates a solvus at 600°C suggested from unmixing spinels from the Red Lodge district (Loferski and Lipin, 1983). SG is a solvus calculated from thermodynamics assuming spinels coexisting with Fo_{95} olivine at 600°C (Sack and Ghiorso, 1991). Spinel compositions in the ordinary Iwanai-dake peridotite and chromitite are shown for comparison.

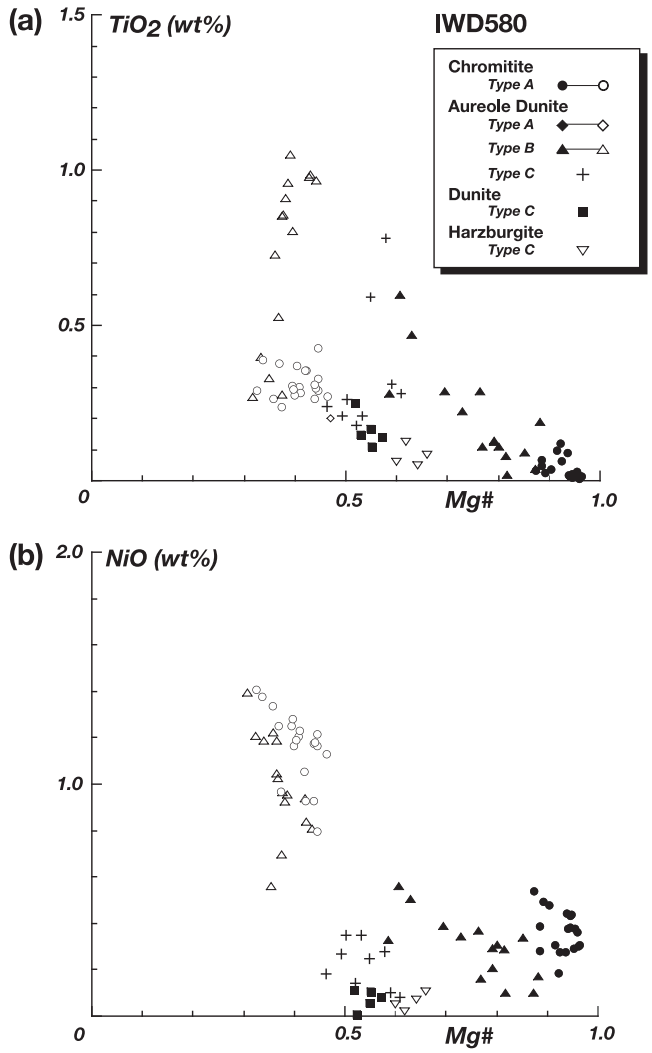

Figure. 6. Chemical compositions of spinel from IWD580 in the Iwanai-dake complex. (a) Variation of Mg# (=Mg/(Mg+Fe^{2+}) atomic ratio) vs TiO_2 content. (b) Variation of Mg# vs NiO content.

content of Type C spinel is 0.10-0.35 wt% in aureole dunite and is <0.11 wt% in surrounding peridotite. We estimated the bulk compositions of Type A and B spinels, based on obtained chemistry and areal ratio of the two phases. The areal ratio was analyzed by using digital images on a public domain Image-J program (website : http : //rsb.info.nih.gov/ij/index.html). The bulk spinel compositions are listed in Table 2 and plotted in Figures 4 and 5b. The variation of Fo content of coexisting olivine from the chromitite layer to surrounding peridotites is shown in Figure 3. The Fo content tends to decrease from the chromitite layer (Fo_{95-96}) to surrounding dunite and harzburgite (Fo_{91-92}). Olivine in aureole dunite is Fo_{92-94}.

Table. 2. Estimated bulk spinel compositions of Type A and B spinel, and areal ratios between contiguous phases. The composition for Type A is an average of 8 domains in a chromitite thin section (MF22). 2s : standard deviation at the 2 sigma. The compositions for Type B are from representative two spinel grains.

	TYPE A		TYPE B	
Sample #	MF22		MF6	MF7
Lithology	Chromitite		Aureole	Aureole
Area Ratio		2s		
Light Phase	88.4%	5.8%	68.8%	47.2%
Dark Phase	11.6%	-	31.2%	52.8%
Bulk Spinel				
SiO_2	0.00	0.01	0.02	0.01
TiO_2	0.26	0.04	0.28	0.71
Al_2O_3	8.74	3.28	18.98	15.93
Cr_2O_3	2.63	0.66	10.04	21.78
Fe_2O_3	60.41	3.40	42.51	33.15
FeO	16.91	1.34	16.12	16.67
MnO	0.17	0.03	0.23	0.37
MgO	9.89	1.12	11.85	11.12
NiO	1.10	0.07	0.98	0.65
Total	100.15	0.91	101.04	100.44
Si	0.000	0.000	0.000	0.000
Ti	0.007	0.001	0.007	0.018
Al	0.277	0.092	0.608	0.594
Cr	0.071	0.018	0.253	0.554
Fe3+	1.627	0.095	1.113	0.819
Fe2+	0.506	0.044	0.464	0.455
Mn	0.005	0.001	0.007	0.010
Mg	0.480	0.045	0.523	0.530
Ni	0.031	0.002	0.027	0.017
Mg#	0.486	0.045	0.528	0.538
Cr#	0.424	0.087	0.458	0.507
Cr/	0.036	0.009	0.128	0.282
Al/	0.139	0.046	0.306	0.301
Fe3+/3+	0.825	0.048	0.566	0.417
Fe3+/Fet	0.763	0.008	0.678	0.634

6. Discussion

Miscibility gap of spinel has been documented by both experimental and thermodynamic studies (e.g., Turnock and Eugster 1962 ; Sack and Ghiorso 1991). Inhomogeneous spinels due to immiscibility have been well described from some metamorphosed ultramafic and mafic rocks (Muir and Naldrett 1973 ; Loferski and Lipin 1983 ; Lipin 1984 ; Eales et al. 1988 ; Zakrezewski 1989 ; Burkhard 1993). Compositional relationships of IWD580 spinels strongly suggest that the inhomogeneous textures in spinel are caused by unmixing due to miscibility gap. Loferski and Lipin (1983) interpreted the inhomogeneity of spinel in meta-gabbro from the Red Lodge Mountain, Montana, as unmixing of Fe-rich and Al-rich phases representing a miscibility gap. They have shown a solvus of spinel in terms of trivalent cations (Cr-Al-Fe^{3+}) at a temperature of approximately 600°C (Fig. 5b).

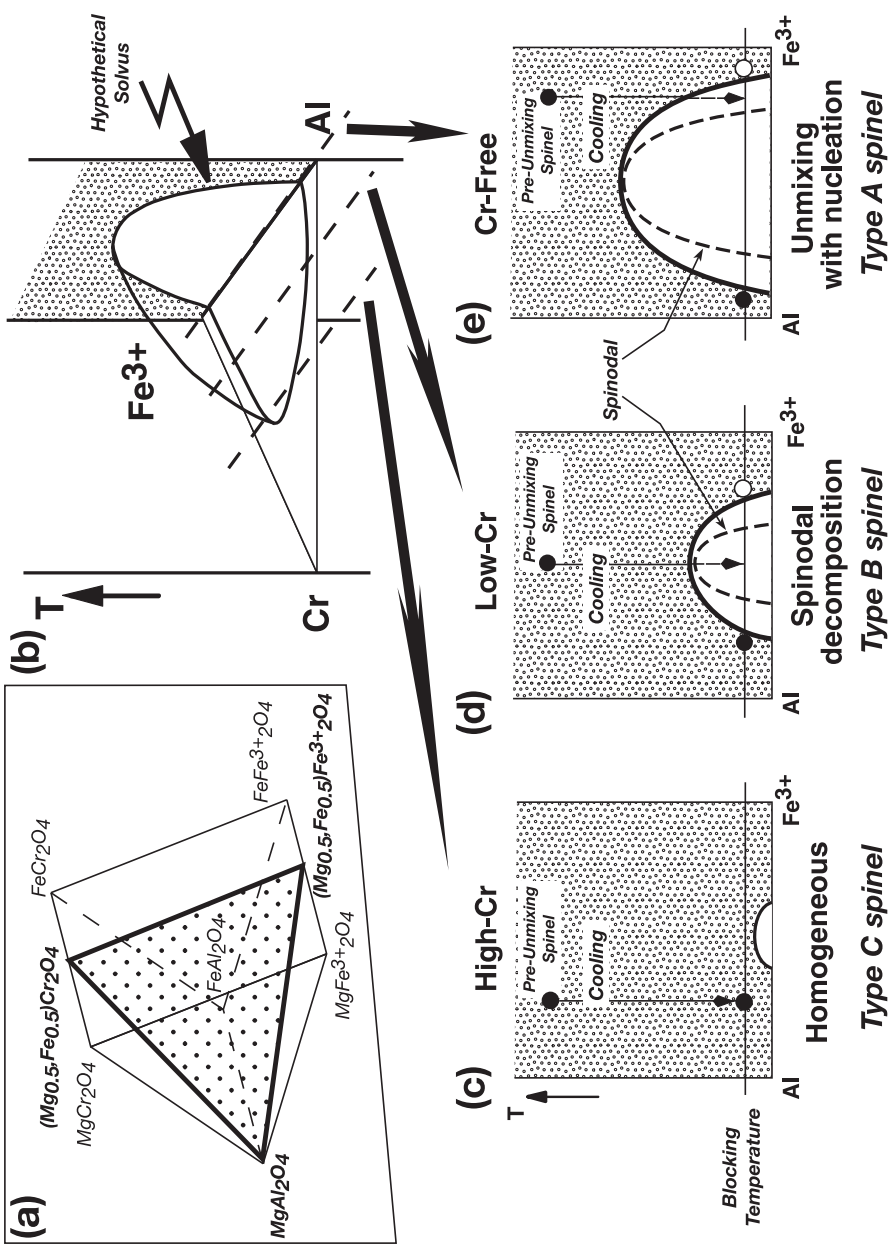

Figure. 7. Schematic diagram for interpretation of relationships between unmixing texture and chemical composition in spinel from IWD580. (a) The spinel prism and approximate plane for IWD580 spinel compositions (cf. Figures 5 and 6). (b) Hypothetical solvus in the T-trivalent cations (Cr-Al-Fe^{3+}) space. The solvus is estimated from Sack and Ghiorso (1991). (c) (d) (e) Al-Fe^{3+} binary planes cut through the iso-Cr ratio planes of (b). Each plane labeled by Cr-free, low-Cr and high-Cr corresponds to Type A, B and C spinel, respectively (See text).

An expected solvus of IWD580 is slightly different in shape from the solvus shown by Loferski and Lipin (1983) (Fig. 4b). This is due to a difference of Mg# of spinel. The immiscible field on the spinel prism may decrease from the Fe-rich side to the Mg-rich side (Fig. 7 of Loferski and Lipin, 1983). The temperature should be also a factor controlling the immiscible field. Sack and Ghiorso (1991) showed differences in solvus at different temperatures and compositions based on thermodynamic calculations (Fig. 5b). We estimated the equilibrium temperature of IWD580 section. For the chromitite and surrounding peridotite, 710-900°C is calculated using calibration of Ballhaus et al. (1991). Arai (1978) estimated the equilibrium temperature of the Iwanai-dake peridotite, based on the olivine-spinel geothermometer (Evans and Frost, 1975), to be 700°C or higher. Spinel unmixing is a function of composition and temperature : Fe^{3+}-rich spinel compositions inside the apparent immiscible field in terms of the trivalent cation ratio (Fig. 5b) is common in differentiated gabbros and altered alpine-type peridotites. Lipin (1984) reported spinel with unmixing textures from alpine-type peridotite. The unmixing may have been caused by high-temperature regional metamorphism after serpentinization during or after emplacement (Lipin, 1984). On the other hand, peridotites from the Iwanai-dake complex are almost free from serpentinization and have no evidence of deserpentinization. The Iwanai-dake peridotite and IWD580 chromitite have probably undergone neither regional metamorphism nor serpentinization after emplacement. Therefore, the inhomogeneous texture was obtained during a cooling process of the mantle peridotite upon emplacement. We conclude that the inhomogeneous texture observed was formed by unmixing during cooling to about 700°C indicated by Mg-Fe partitioning between olivine and spinel.

The variety of textures in Type A and B spinels (unmixed) and Type C spinel (homogeneous) can be interpreted by differences of initial spinel composition because the textural variation is systematically related with the chemical composition. It is postulated that pre-unmixing spinel composition is represented by estimated bulk spinel composition of unmixing spinel (Table. 2). Let us consider the processes on an ideal phase diagram of spinel (Fig. 7). Each spinel phase and pre-unmixing spinel composition from IWD580 can be approximated on a plane, $(Mg_{0.5},Fe^{2+}_{0.5})Cr_2O_4$-$MgAl_2O_4$-$(Mg_{0.5},Fe^{2+}_{0.5})Fe^{3+}_2O_4$, in the spinel prism, and we draw a hypothetical solvus on the plane of trivalent cations (Cr-Al-Fe^{3+}) (Fig. 7a, b). Type C spinel represented by high-Cr spinel is free from unmixing, which suggests that this composition is outside of solvus at the blocking temperature (Fig. 7c). According to Sack and Ghiorso (1991), Type A and B spinels must be single phases as solid solutions at high temperature (>900°C). In Figure 7, the pre-unmixing spinel compositions of Type A and B represent, on the binary system, low-Cr and Cr-free compositions, respectively (Fig. 7d, e). Both compositions enter the immiscible field during cooling. In Type A spinel dark-colored granules (e.g., Plate I-d, e) could be effectively formed by phase separation of nucleation growth. The pre-unmixing spinel composition of Type A spinel, of which $MgAl_2O_4$ component is very small in amount relative to $(Mg_{0.5},Fe^{2+}_{0.5})$ $Fe^{3+}_2O_4$ component (Fig. 7e), causes discontinuous transformation. This process forms nucleus of $MgAl_2O_4$,

dark-colored granules observed. On the other hand, Type B spinel does not show nucleation (e.g., Plate II-g, III-d). Pre-unmixing composition of Type B spinel could correspond to inside of spinodal at the blocking temperature (Fig. 7d). Thus we can ascribe the symplectic texture in Type B spinel to the spinodal decomposition of continuous transformation (e.g., Kingery et al., 1976). The textural variations between Types A, B and C were possibly due to gradual differences of pre-unmixing spinel composition but not to the differences of cooling rate or thermal history.

Unmixing textures of IWD580 spinel are various, speckled or irregular symplectic texture as shown above, but do not show trellis lamellae texture commonly observed in ilmenite-magnetite unmixing (e.g., Haggerty, 1991a). We speculate that this difference is due to the difference of crystal system of unmixing phases. Ilmenite and magnetite belong to the hexagonal and cubic systems, respectively. Thus the trellis lamellae texture is probably developed by an anisotropic feature of ilmenite. On the other hand, both phases in IWD580 unmixing spinel belong to the cubic system. They are isotropic and non-crystallographic-controlled texture should be developed during unmixing.

7. Conclusions and suggestions for further study

Compositional relationship between two spinel phases in this study supports that the inhomogeneous texture in spinel was developed by unmixing process due to immiscibility at low temperature. The textural variety of unmixing spinel is dependent on composition of initial pre-unmixing spinel.

If the estimated pre-unmixing composition is appropriate, then a next problem may arise on the origin of the pre-unmixing spinel. The pre-unmixing spinel composition is much higher in ferric iron content than spinel from mantle derived peridotite and chromitite ever reported not only from the Iwanai-dake complex (Fig. 5b) but also from the world (e.g., Arai and Yurimoto, 1995 ; Zhou et al., 1996 ; Melcher et al., 1997). We suspect that a highly oxidized melt had played an important role in the IWD580 chromitite formation. Because the chromitite formation has been attributed to reaction between mantle peridotite and melt (e.g., Arai and Yurimoto, 1994 ; Zhou et al, 1994), and the spinel composition strongly depends on oxygen fugacity in crystallization (e.g. Hill and Roeder, 1974). We also focus on the irregularity of unmixing texture observed. For example, Type B spinel grain contains two portions with symplectic texture and homogeneous appearance (e.g., Plate. III-b, IV-d). This may be due to initial chemical heterogeneity within the pre-unmixing spinel phase.

Acknowledgments

We would like to give special thanks to M. Makita and K. Kadoshima for their help in field survey and collecting rocks. A. Toramaru and A. Tsune are gratefully acknowledged for daily discussion and helpful suggestions. A. Ishiwatari and T. Morishita are thanked for

constructive comments. Y. Shimizu is thanked for assistance with the electron microprobe. Hatanaka Co. kindly allowed us the field survey in the quarry.

Reference

Arai, S. (1978) Chromian spinel lamellae in olivine from the Iwanai-dake peridotite mass, Hokkaido, Japan. *Earth Planet. Sci. Lett*., v. 39, p. 267-273.

Arai, S. (1987) An estimation of the least depleted spinel peridotite on the basis of olivine-spinel mantle array. *N. Jb. Miner. Mh*., v. 8, p. 347-354.

Arai, S. (1994) Characterization of spinel peridotites by olivine-spinel compositional relationships : Review and interpretation. *Chem. Geol*., v. 113, p. 191-204.

Arai, S. and Hirai, H. (1985) Relics of H_2O fluid inclusions in mantle-derived olivine. *Nature*, v. 318, p. 276-277.

Arai, S., and Yurimoto, H. (1994) Podiform chromitites of the Tari-Misaka ultramafic complex, Southwestern Japan, as mantle-melt interaction products. *Economic Geology*, v. 89, p. 1279-1288.

Asahina, T. and Komatsu, M. (1979) The Horokanai ophiolitic complex in the Kamuikotan Tectonic Belt, Hokkaido, Japan. *Jour. Geol. Soc. Japan*, v. 85, p. p. 317-330.

Ballhaus, C., Berry, R. F. and Green, D. H., (1991). High pressure experimental calibration of the olivine -orthopyroxene-spinel oxygen geobarometer : implications for the oxidation state of the upper mantle. *Contrib. Mineral. Petrol*., v. 107, 27-40.

Bamba, T. (1955) Petrological study on the Iwanaidake peridotite mass. *Bull. Geol. Committ. Hokkaido*, v. 29, p. 7 (in Japanese).

Bloomer, S.H. and Fisher, R.L. (1987) Petrology and geochemistry of igneous rocks from the Tonga Trench-A non-accreting plate boundary. *Jour. Geol*., v. 95, p. 469-495.

Bloomer, S.H. and Hawkins, J.W. (1983) Gabbroic and ultramafic rocks from the Mariana trench : an island arc ophiolite. In : D.E. Hayes (Ed.) *The Tectonics and Geologic Evolution of Southeast Asian Seas and Islands : Part II. Geophys. Monogr*., American Geophysical Union, v. 27, p. 294-317.

Burkhard, D.J.M. (1993) Accessory chromium spinels : Their coexistence and alteration in serpentinites. *Geochim. Cosmochim. Acta*, v. 57, p. 1297-1306.

Cremer, V. (1969) Die Mischkristallbildung im System Chromit-Magnetit-Hercynit zwischen 1000 und 500° C. *N. Jb. Mineral. Abh*., v. 111, p. 184-205 (in German with English abstract).

Dick, H.J.B. and Bullen, T. (1984) Chromian spinel as a petrogenetic indicator in abyssal and alpine-type peridotites and spatially associated lavas. *Contrib. Mineral. Petrol*., v. 86, p. 54-76.

Eales, H.V., Wilson, A.H. and Reynolds, I.M. (1988) Complex unmixed spinels in layered intrusions within an obducted ophiolite in the Natal-Namaqua mobile belt. *Mineral. Deposita*, v. 23, p. 150-157.

Evans, B.W., and Frost, B.R. (1975) Chrome-spinel in progressive metamorphism a preliminary analysis. *Geochim. Cosmochim. Acta*, v. 39, 959-972.

Haggerty, S.E. (1991a) Oxide textures-a mini-atlas. In D.H. Lindsley, (Ed.) *Oxide Minerals : Petrologic and Magnetic Significance. Reviews in Mineralogy*, Mineralogical Society of America, Washington,

D.C., v. 25, p. 129-219.

Haggerty, S.E. (1991b) Oxide mineralogy of the upper mantle. In : D.H. Lindsley, (Ed.) *Oxide Minerals : Petrologic and Magnetic Significance. Reviews in Mineralogy*, Mineralogical Society of America, Washington, D.C., v. 25, p. 355-416.

Hill, R., and Roeder, P. (1974) The crystallization of spinel from basaltic liquid as function of oxygen fugacity. *Jour. Geol*., v. 82, p. 709-729.

Hirai, H. and Arai, S. (1987) H_2O-CO_2 fluids supplied in alpine-type mantle peridotites : electron petrology of relic fluid inclusions in olivines. *Earth Planet. Sci. Lett*., v. 85, p. 311-318.

Irvine, T.N. (1965) Chromian spinel as a petrognetic indicator. Part 1. Theory. *Can. Jour, Earth Sci*., v. 2, p. 648-672.

Ishii, T., Robinson, P.T., Maekawa, H. and Fiske, R. (1992) Petrological studies of peridotites from diapiric serpentinite seamounts in The Izu-Ogasawara-Mariana forearc, LEG125. In : P. Fryer, J.A. Pearce, L.B. Stokking et al., (Eds). *Proc. ODP, Sci. Results*, College Station, Texas (Ocean Drilling Program), v. 125, p. 445-485.

Ishizuka, H. (1980) Geology of the Horokanai Ophiolite in the Kamuikotan Tectonic Belt, Hokkaido, Japan. *Jour. Geol. Soc. Japan*, 86, p. 119-134 (in Japanese with English abstract).

Ishizuka, H., Imaizumi, M., Gouchi, N. and Banno, S. (1983) The Kamuikotan zone in Hokkaido, Japan : Tectonic mixing of high-pressure and low-pressure metamorphic rocks. *Jour. Metamor. Geol*., v. 1, p. 263-275.

Katoh, T. (1978) The Sarugawa ultrabasic massif in Kamuikotan belt, central axial zone of Hokkaido. *Earth Science (Chikyu Kagaku)*, v. 32, p. 273-279 (in Japanese with English abstract).

Katoh, T. and Nakagawa, M. (1986) Tectogenesis of ultramafic rocks in the Kamuikotan tectonic belt, Hokkaido, Japan. *Monogr. Assoc. Geol. Collab. Japan*, v. 31, p. 119-135 (in Japanese with English abstract).

Kingery, W.D., Bowen, H.K., and Uhlmann, D.R. (1976) *Introduction to Ceramics*, 2nd edition. A Wiley-Ineterscience Publication, New York. 1056 p

Kubo, K. (2002) Dunite formation processes in highly depleted peridotite : case study of the Iwanaidake peridotite, Hokkaido, Japan. *Jour. Petrol*., v. 43, p. 423-448.

Lipin, B.R. (1984) Chromite from the Blue Ridge Province of North Carolina. *Am. Jour. Sci*., v. 284, p. 507-529.

Loferski, P.J. and Lipin, B.R. (1983) Exsolution in metamorphosed chromite from the Red Lodge district, Montana. *Am. Mineral*., v. 68, p. 777-789.

Melcher, F., Grum, W., Simon, G., Thalhammer, T.C., and Stumpfl, E.F. (1997) Petrogenesis of the ophiolitic giant chromite deposits of Kempirsai, Kazakhstan : a study of solid and fluid inclusions in chromite. *Jour. Petrol*., v. 36, p. 1419-1458.

Mercier, J.C. and Nicolas, A. (1975) Textures and fabrics of upper mantle peridotites as illustrated by xenoliths from basalt. *Jour. Petrol*., v. 16, p. 454-487.

Miyashiro, A. (1961) Evolution of Metamorphic Belts. *Jour. Petrol*., v. 2, p. 227-331.

Muir, J.E. and Naldrett, A.J. (1973) A natural occurrence of two-phase chromium-bearing spinels. *Can. Mineral*., v. 11, p. 930-939.

Niida, K. and Katoh, T. (1978) Ultramafic rocks in Hokkaido. *Monogr. Assoc. Geol. Collab. Japan*, v. 21, p. 61-81 (in Japanese with English abstract).

Parkinson, I.J. and Pearce, J.A. (1998) Peridotites from the Izu-Bonin-Mariana forearc (ODP Leg 125) : evidence for mantle melting and melt-mantle interaction in a supra-subduction zone setting. *Jour. Petrol*., v. 39, p. 1577-1618.

Sack, R.O. and Ghiorso, M.S. (1991) Chromian spinels as petrogenetic indicators : Thermodynamics and petrological applications. *Am. Mineral*., v. 76, 827-847.

Tamura, A., Makita, M. and Arai, S. (1999) Petrogenesis of ultramafic rocks in the Kamuikotan belt, Hokkaido, northern Japan. *Memoir. Geol. Soc. Japan*, v. 52, p. 53-68 (in Japanese with English abstract).

Turnock, A.C. and Eugster, H.P. (1962) Fe-Al oxides : Phase relationships below 1000°C. *Jour. Petrol*., v. 3, p. 533-565.

Zakrezewski, M.A. (1989) Chromian spinels from Kusa, Bergslagen, Sweden. *Am. Mineral*., v. 74, p. 448-455.

Zhou, M.F., Robinson, P.T., and Bai, W.J. (1994) Formation of podiform chromitites by melt/rock interaction in upper mantle. *Mineral. Deposita*, v. 29, 980-101.

Zhou, M.-F., Robinson, P.T., Malpas, J., and Li, Z. (1996) Podiform chromitites in the Luobusa ophiolite (southern Tibet) : implications for melt-rock interaction and chromite segregation in the upper mantle. *Jour. Petrol*., v. 37, 3-21.

PLATES

Mode of occurrence of IWD580 chromitite and the textural variety of spinel. Sample MF22 is from chromitite layer, samples MF6, 7, 22 and 23 are from aureole dunite and sample MF1 and 3 are from surrounding peridotite (see Fig. 3).

Plate I (Outcrop and MF22)

(a) and (b) An outcrop of IWD580 in the Iwanai-dake complex.
(a) The chromitite layer (black) pinches out at left side.
(b) Subhedral olivine (grey dots) in chromitite layer (black) and spinel concentration in aureole dunite.
(c) Photomicrograph of massive spinel (black) in MF22. White dots in spinel are yellow or green in color. Plane-polarized light.
(d) Reflected-light photomicrograph of (c). Note that some dark-colored granules correspond to white dots in (c).
(e)-(h) Photomicrographs in reflected light.
(e) Granules (grey) and host (white) are spinel *sensu stricto* and Mg-rich magnetite in composition, respectively. Granules are distributed irregularly but often show linear or concentric arrays.
(f)-(h) Close up of (e). Note that the granules are various in size. Stars in (e) to (h) indicate the same position for reference. Spinel with this inhomogeneous texture in MF22 is classified as Type A.

Plate II (MF 6)

Reflected-light photomicrographs of spinel in MF6. The pictures are arranged from (a) to (h) from the chromitite side outward. (a) to (d) show textures of Type A spinel and the others show those of Type B spinel.
(a) and (b) Speckled texture in subhedral spinel.
(c) Speckled texture is predominant but irregular texture exists at the rim .
(d) Close-up of (c)
(e) Irregular mottling texture. Note that light-colored phase is predominant.
(f) Close-up of (e) showing a dark-colored phase at the rim.
(g) Fine irregular mottling texture.
(h) Close-up of (g) showing the symplectic texture at the rim.

Plate III (MF 7)

Reflected-light photomicrographs of spinel in MF7. The pictures are arranged from (a) to (h) in order of distance from chromitite. (a) to (g) exhibit Type B spinel pattern and (h) is the Type C spinel texture.
(a) Irregular mottling texture. Note the irregular shape of the dark-colored phase.
(b) Irregular mottling texture. Note the dark-colored phase at the rim.
(c) Mottling and symplectic texture distributed irregularly. Note that the light-colored phase is predominant
(d) Close-up of (c)
(e) Symplectic texture existing between light-and dark-colored parts with homogeneous appearance. Note that the dark-colored phase is predominant.
(f) Close-up of (e) showing gradual transition from symplectic texture to homogeneous texture.
(g) Fine symplectic patten and light-colored appearance at the rim.
(h) Dark-colored homogeneous phase with a light-colored phase at the rim.

Plate IV (MF 23, 24, 1 and 3)

Reflected light photomicrographs of spinel. (a) and (b) show Type A spinel texture, (c) shows Type B spinel texture, and (e) to (h) correspond to Type C spinel.
(a) and (b) Speckle texture in spinel aggregates from aureole dunite (MF23).
(c) Symplectic texture between light-and dark-colored homogeneous phases (MF24).
(d) A close-up of (c).
(e) and (f) Homogeneous-looking spinel in MF24. Note the light-colored phase only exists as spot and rim.
(g) and (h) Homogeneous spinel in MF1 and MF3, respectively.

Plate I (Outcrop and MF22)

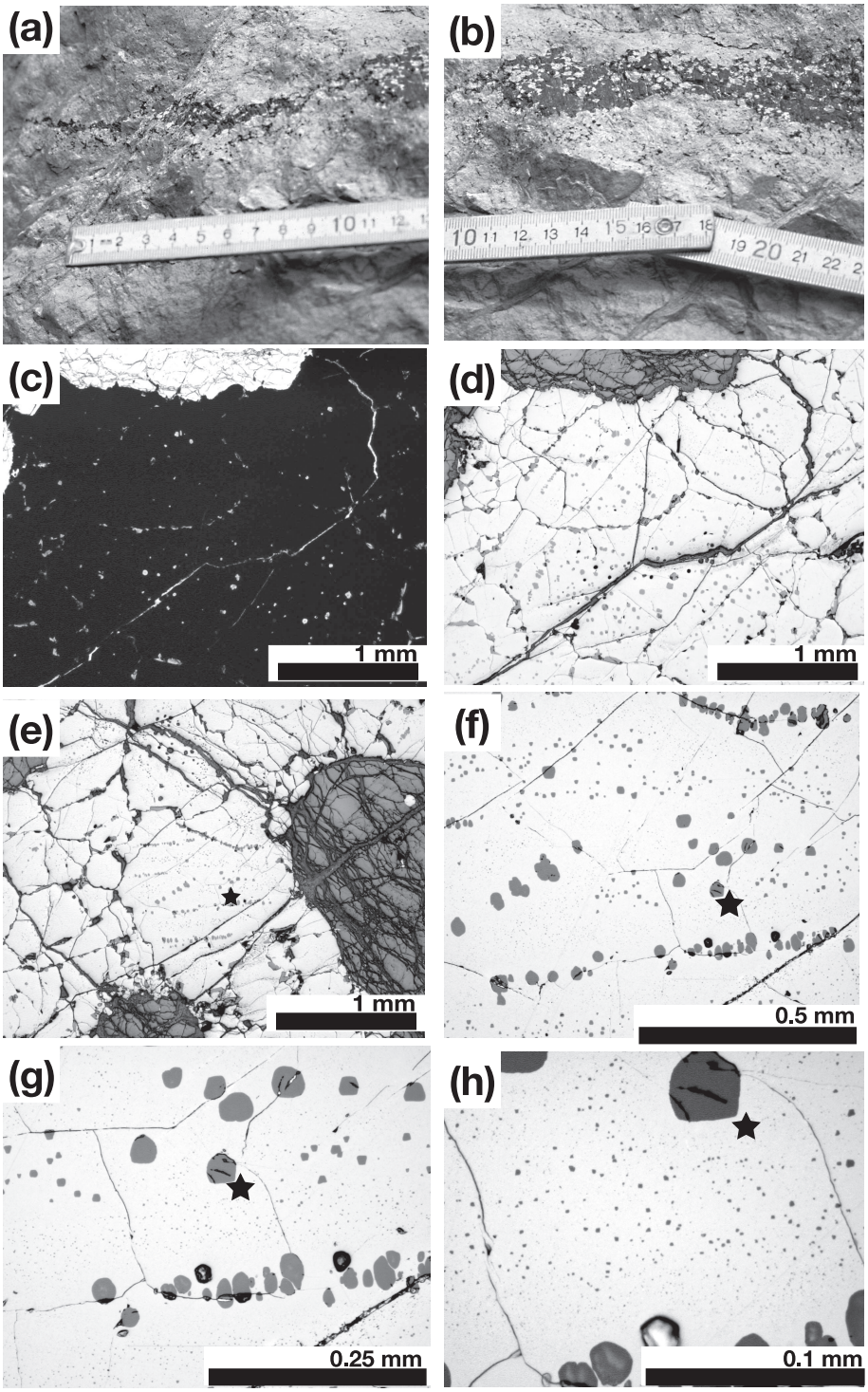

Plate II (MF 6)

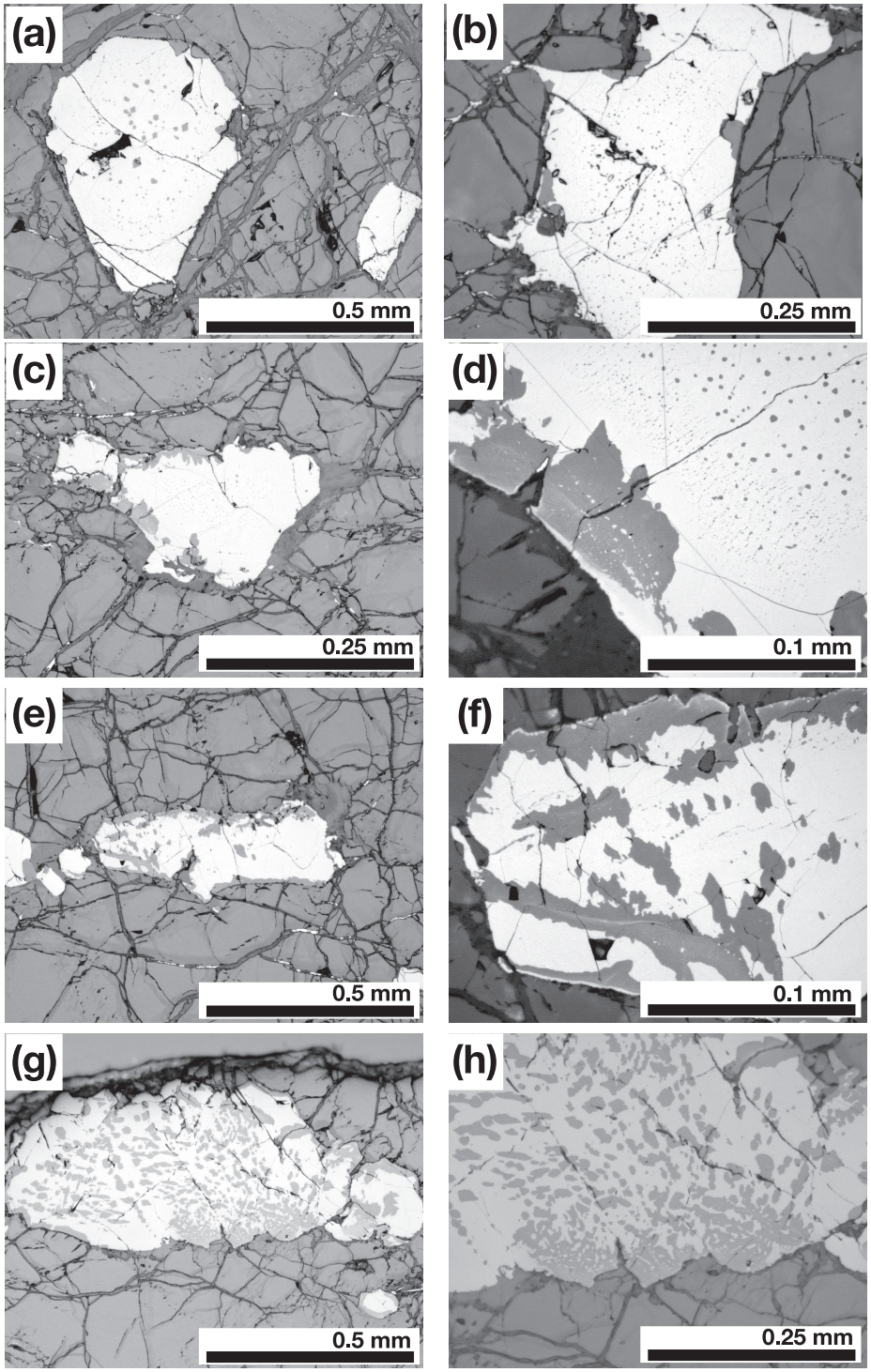

Plate III (MF 7)

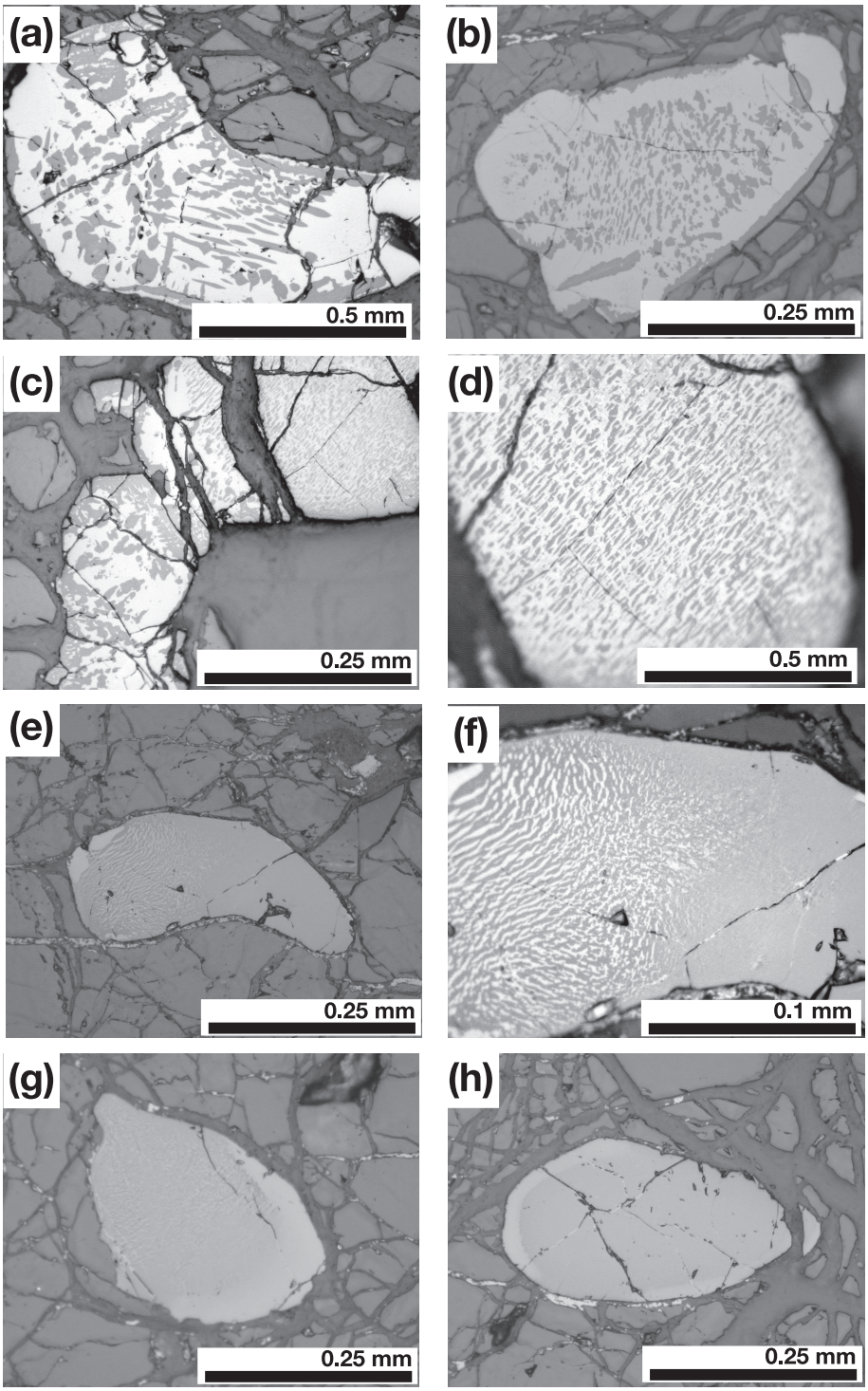

Plate IV (MF 23, 24, 1 and 3)